JCI insight

RESEARCH ARTICLE

Loss of *Wasl* improves pancreatic cancer outcome

Ana Hidalgo-Sastre,[1] Judit Desztics,[1] Zahra Dantes,[1] Katharina Schulte,[1] Hilal Kabadayi Ensarioglu,[1,2] Blessing Bassey-Archibong,[3] Rupert Öllinger,[1,4] Thomas Engleiter,[1,4] Lyndsay Rayner,[3] Henrik Einwächter,[1] Juliet M. Daniel,[3] Ali Sameer Abdulghani Altaee,[1] Katia Steiger,[5] Marina Lesina,[1] Roland Rad,[1,4] Maximilian Reichert,[1] Guido von Figura,[1] Jens T. Siveke,[6,7,8] Roland M. Schmid,[1,7] and Clara Lubeseder-Martellato[1]

[1]KIinik und Poliklinik für Innere Medizin II, Technical University of Munich, Germany. [2]Department of Histology and Embryology, Manisa Celal Bayar University, Turkey. [3]Department of Biology, McMaster University, Hamilton, Ontario, Canada. [4]Institute of Molecular Oncology and Functional Genomics and [5]Institute of Pathology, Technical University of Munich, Munich, Germany. [6]Institute for Developmental Cancer Therapeutics, West German Cancer Center, University Hospital Essen, Essen, Germany. [7]Division of Solid Tumor Translational Oncology, German Cancer Consortium (DKTK) partner site Essen, Essen, Germany. [8]German Cancer Research Center (DKFZ), Heidelberg, Germany.

Several studies have suggested an oncogenic role for the neural Wiskott-Aldrich syndrome protein (N-WASP, encoded by the *Wasl* gene), but thus far, little is known about its function in pancreatic ductal adenocarcinoma (PDAC). In this study, we performed in silico analysis of *WASL* expression in PDAC patients and found a correlation between low *WASL* expression and prolonged survival. To clarify the role of *Wasl* in pancreatic carcinogenesis, we used 2 oncogenic *Kras*–based PDAC mouse models with pancreas-specific *Wasl* deletion. In line with human data, both mouse models had an increased survival benefit due to either impaired tumor development in the presence of the tumor suppressor *Trp53* or the delayed tumor progression and senescent phenotype upon genetic ablation of *Trp53*. Mechanistically, loss of *Wasl* resulted in cell-autonomous senescence through displacement of the N-WASP binding partners WASP-interacting protein (WIP) and p120ctn; vesicular accumulation of GSK3β, as well as YAP1 and phosphorylated β-catenin, which are components of the destruction complex; and upregulation of *Cdkn1a(p21)*, a master regulator of senescence. Our findings, thus, indicate that *Wasl* functions in an oncogenic manner in PDAC by promoting the deregulation of the p120-catenin/β-catenin/p21 pathway. Therefore, strategies to reduce N-WASP activity might improve the survival outcomes of PDAC patients.

Introduction

Activating mutations of the *Kras* oncogene are the driver mutations for pancreatic ductal adenocarcinomas (PDACs), which is one of, if not the, most lethal human cancer with a 5-year survival rate under 5% (1). In addition to *Kras*-activating mutations, several genetic alterations, such as inactivation of the tumor suppressor genes *Trp53* and *Cdkn2a(p16)*, also accumulate during the malignant transformation of the pancreas (2), which accelerates the progression of PDAC. Several studies suggest that PDAC develops through preneoplastic lesions originating from acinar-to-ductal metaplasia (ADM) (3–5). We previously showed that ADM depends on an increase in fluid-phase endocytosis (6) — a receptor-independent endocytic pathway characterized by fluid phase markers as cargos. We further showed that this ADM is dependent on the neural Wiskott-Aldrich syndrome protein (N-WASP, encoded by the *Wasl* gene). N-WASP is an indicator of poor prognosis in several cancers and has been implicated in the regulation of metastasis via the promotion of cell migration and remodeling of the extracellular matrix (6–11). At the cellular level, N-WASP interacts with components of the actin cytoskeleton, including the ARP2/3 complex and CDC42, as well as with PIP2 (12, 13). Notably, actin polymerization has been shown to be crucial for PDAC development, and both CDC42 and PIP2 are effectors of KRAS (14–16). N-WASP further interacts through its VCA and WH1 domains with p120-catenin (p120ctn) and the WASP-interacting protein (WIP), respectively (12, 13), both of which were recently implicated in PDAC aggressiveness and progression (17–19). Therefore, N-WASP may function as a driver for PDAC development and progression. However, little is known about

Authorship note: AHS, JD, ZD, and KS contributed equally to this work.

Conflict of interest: The authors have declared that no conflict of interest exists.

Submitted: January 9, 2019
Accepted: April 22, 2020
Published: May 21, 2020.

Reference information: *JCI Insight*. 2020;5(10):e127275. https://doi.org/10.1172/jci.insight.127275.

the role of N-WASP in PDACs. Taking advantage of the reproducible kinetics of tumor formation in mouse models of PDAC, we investigated the role of N-WASP expression in pancreatic cancer development and progression using genetic and molecular approaches.

Herein, we show that *Wasl* deletion in 2 mouse models of PDAC driven by oncogenic *Kras* leads to a survival benefit. Similarly, patients stratified for low *WASL* expression showed improved survival, underlying the relevance of the murine model to the human disease. *Wasl* deletion impaired tumor development in the presence of the tumor suppressor *Trp53* and led to delayed tumor progression in the absence of *Trp53*. The biallelic loss of *Wasl* in the latter model also led to cell-autonomous senescence in pancreatic tumor cells characterized by Senescence-associated–β-galactosidase (SA–β-galactosidase) activity and *Cdkn1a(p21)* upregulation. We also show a displacement of the N-WASP binding partners WIP and p120ctn upon deletion of *Wasl*, which resulted in increased endocytosis — linked to accumulation of the components of the β-catenin destruction complex YAP1 and dephosphorylated, inactive β-catenin in tumor cells. The induction of nuclear p120ctn combined with the inhibition of endocytosis rescued the senescent phenotype observed in *Wasl*-depleted cells. This suggests that *Wasl* functions, in part, in PDAC development by regulating p120ctn localization and by inhibiting endocytosis. Overall, this study demonstrates a tumor-promoting role for *Wasl* in PDAC development via regulation of protein stability and subcellular localization of components of the p120ctn/β-catenin signaling pathway.

Results

Wasl is involved in PDAC outcome. *Wasl*, encoding for N-WASP, is upregulated in both human and mouse PDAC models (6, 7) and has primarily been associated with enhanced tumor invasion. To determine the clinical relevance of *Wasl* in human PDAC, we stratified human PDAC samples for low and high *WASL* expression, and we observed a correlation between low *WASL* expression and increased survival in PDAC patients (Figure 1A). To better understand the function of *Wasl* in PDAC, we generated a pancreatic conditional *Wasl*-KO mice in the *Ptf1a*$^{Cre/+}$ *Kras*$^{LSL\text{-}G12D/+}$ mouse model of PDAC (20) to generate *Ptf1a*$^{Cre/+}$ *Kras*$^{LSL\text{-}G12D/+}$ *Wasl*$^{\Delta Panc}$ mice (hereafter CK and CK-N$^{\Delta Panc}$ mice, respectively). At 4 weeks of age, CK-N$^{\Delta Panc}$ pancreata showed large areas of edema, with infiltrating cells and fatty metaplasia, while CK mice pancreata exhibited large areas with acinar tissue and focal metaplastic lesions (Figure 1, B and D). Consistent with the gross phenotype, CK-N$^{\Delta Panc}$ mice displayed an increase in the amount of pancreatic fat (Figure 1D) and an impressive infiltration of F4/80-positive macrophages, along with mast cells (Figure 1C and Supplemental Figure 1, A and B; supplemental material available online with this article; https://doi.org/10.1172/jci.insight.127275DS1). These results were reminiscent of a pancreatitis-like phenotype. Notably, the infiltrating macrophages decreased with age, reaching a level below that present in the control terminal CK mice (Supplemental Figure 1B). In agreement with the inflammatory phenotype, CK-N$^{\Delta Panc}$ expressed REG3A (Supplemental Figure 1C), which is upregulated during pancreatitis and is involved in ADM (21); CK-N$^{\Delta Panc}$ also expressed high active β-catenin levels, which is activated during pancreatitis (22) (Supplemental Figure 1, D and E). However, CK-N$^{\Delta Panc}$ mice do not develop ADM at 3 months of age (6), which led us to conclude that lack of *Wasl* blocks ADM downstream of REG3A and β-catenin. To unravel the molecular effect of *Wasl* depletion, we performed RNA sequencing (RNAseq) of the pancreata of 4-week-old CK and CK-N$^{\Delta Panc}$ mice. The differentially expressed genes with an adjusted P value of < 0.02 (Supplemental Table 1) were subjected to gene set enrichment analysis using the program Enrichr (23, 24). In agreement with our histological data, CK-N$^{\Delta Panc}$ pancreatic tissues displayed an enrichment of genes involved in pancreatitis and the immune system (Figure 1E and Supplemental Table 2) and a downregulation of genes involved in the DNA replication pathway (Figure 1E and Supplemental Table 2). Notably, pancreatitis induces injury of acinar cells that has been described to lead to fatty degeneration (25), which may explain the observed fatty metaplasia. Gene Set Enrichment Analysis (GSEA; https://www.gsea-msigdb.org/gsea/index.jsp) also revealed an upregulation of adipogenesis and mast cell immunity, which were consistent with the observed "fatty" phenotype seen in the CK-N$^{\Delta Panc}$ mice, as well as an upregulation of inflammatory responses and IL-6 signaling (Figure 1F). In line with the increased amount of active β-catenin expression observed in CK-N$^{\Delta Panc}$ pancreatic tissues, our RNAseq data reveal increased expression of several β-catenin gene targets (Supplemental Table 3), which were validated by reverse transcription PCR (RT-PCR) (Supplemental Figure 1G). Notably, we observed downregulation of the β-catenin target *Myc* in CK-N$^{\Delta Panc}$ pancreatic tissues, along with downregulation of MYC targets, as shown by GSEA (Supplemental Figure 1F and Supplemental Table 3). Since inflammation and IL-6 signaling have been linked

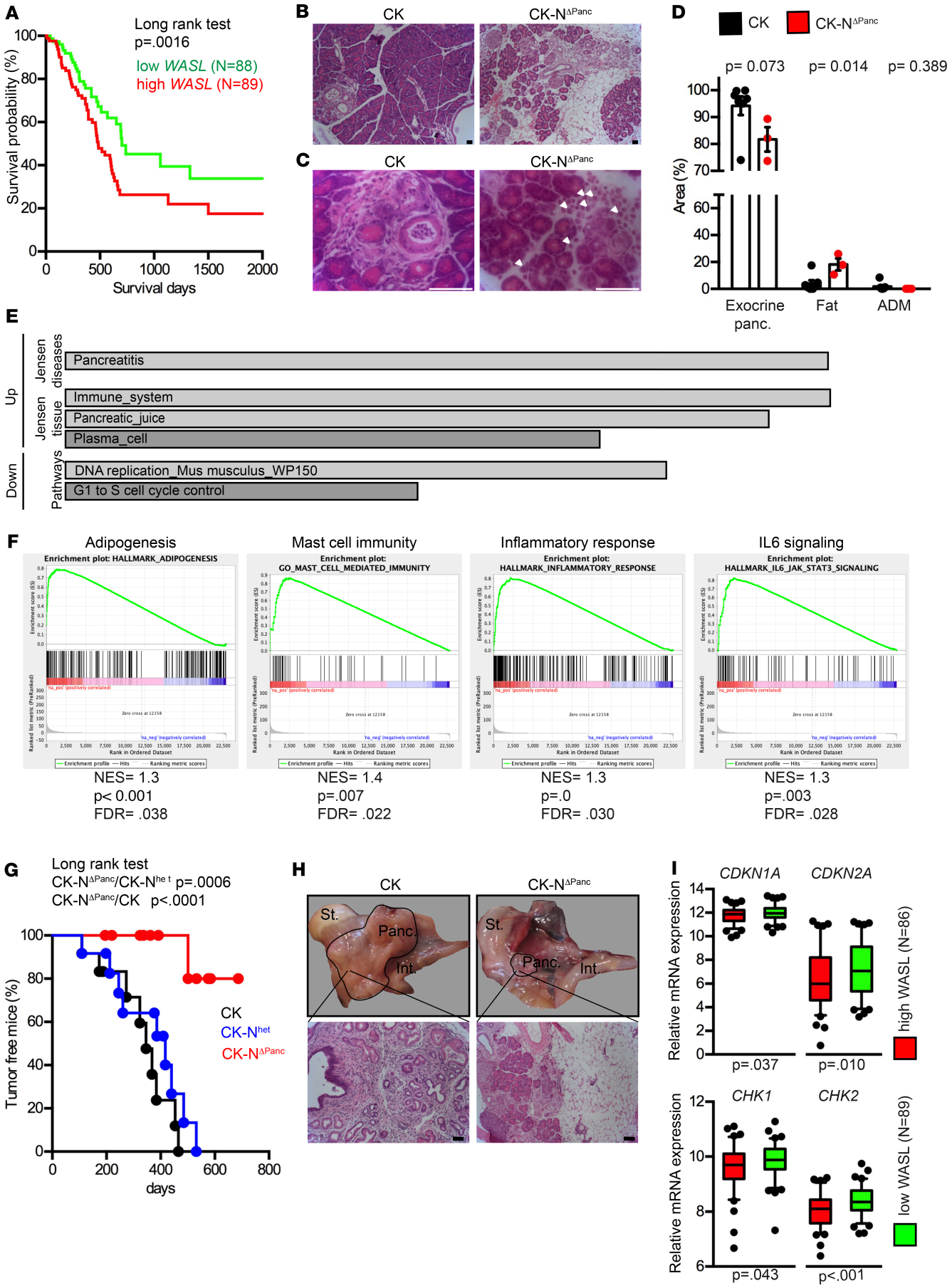
A
Long rank test
p=.0016
low WASL (N=88)
high WASL (N=89)
Survival probability (%)
Survival days
B
CK
CK-NΔPanc
C
CK
CK-NΔPanc
D
CK
CK-NΔPanc
p= 0.073
p= 0.014
p= 0.389
Area (%)
Exocrine panc.
Fat
ADM
E
Up
Jensen diseases
Pancreatitis
Jensen tissue
Immune_system
Pancreatic_juice
Plasma_cell
Down
Pathways
DNA replication_Mus musculus_WP150
G1 to S cell cycle control
F
Adipogenesis
Enrichment plot: HALLMARK_ADIPOGENESIS
NES= 1.3
p< 0.001
FDR= .038
Mast cell immunity
Enrichment plot: GO_MAST_CELL_MEDIATED_IMMUNITY
NES= 1.4
p=.007
FDR= .022
Inflammatory response
Enrichment plot: HALLMARK_INFLAMMATORY_RESPONSE
NES= 1.3
p=.0
FDR= .030
IL6 signaling
Enrichment plot: HALLMARK_IL6_JAK_STAT3_SIGNALING
NES= 1.3
p=.003
FDR= .028
G
Long rank test
CK-NΔPanc/CK-Nhet p=.0006
CK-NΔPanc/CK p<.0001
Tumor free mice (%)
days
CK
CK-Nhet
CK-NΔPanc
H
CK
CK-NΔPanc
St.
Panc.
Int.
I
CDKN1A
CDKN2A
Relative mRNA expression
p=.037
p=.010
high WASL (N=86)
CHK1
CHK2
p=.043
p<.001
low WASL (N=89)

Figure 1. Low *WASL* correlates with improved survival, and loss of *Wasl* in oncogenic *Kras*–driven mouse model for PDAC impairs tumor development. (**A**) Kaplan-Meier survival curve of PDAC patients stratified for *WASL* expression using the UCSC Xena genomic browser. (**B**) Representative H&E staining of pancreata of 4-week-old mice. (**C**) H&E stainings; arrowheads highlight mast cells. Scale bars: 50 μM. (**D**) Morphometric quantification of the amount of ADM lesions, exocrine pancreas, and fat within the pancreatic tissue in 4-week-old animals. CK (n = 7) and CK-N$^{\Delta Panc}$ (n = 3). Data represent mean ± SEM. Student's t test. (**E**) RNAseq was performed from 4 mice per group. The bar graph from the top upregulated and downregulated pathways (combined score: P value multiplied by z score) in 4-week-old CKN$^{\Delta Panc}$ mice. The pathways were obtained after running the differentially regulated genes (n = 155) listed in Supplemental Table 1 through the gene set enrichment program Enrichr. (**F**) Enrichment plots generated by the GSEA tool showing the signatures that were enriched in the CK-N$^{\Delta Panc}$ pancreata. (**G**) Kaplan-Meier tumor-free curves for CK (n = 12), CK-N^{het} (n = 12), and CK-N$^{\Delta Panc}$ (n = 12) mice. (**H**) Upper panels show macroscopic pictures of organs of endpoint mice. Note the tiny pancreas in the CKP-N$^{\Delta Panc}$ mouse. St., stomach; Panc., pancreas; Int., intestine. The lower panels show representative H&E stainings. Scale bars: 50 μM. (**I**) PDAC patients were stratified for *WASL* expression using the UCSC Xena genomic browser, and expression levels of the indicated genes were compared. In the box plots, the whiskers represent the 5th and 95th percentile, and the central line is the median of the data, with the remaining dots being outliers. Unpaired t test with Welch's correction.

to oncogene-induced senescence (OIS) (26, 27) and *Myc* is an essential downstream effector of oncogenic *Kras* in the pancreas (28, 29), and since pancreatitis is a factor promoting PDAC (30, 31), we monitored a cohort of CK-N$^{\Delta Panc}$ mice until endpoint.

CK control mice reproducibly develop PDAC at the age of about 1 year (20), and mice with deletion of 1 *Wasl* allele in this background (hereafter CK-N^{het}) developed tumors at a rate comparable with that of CK mice and with similar survival (Figure 1G and Supplemental Figure1H). Surprisingly, deletion of both *Wasl* alleles impaired tumor development (Figure 1H) and slightly improved survival (Supplemental Figure 1H) compared with CK mice. CK-N$^{\Delta Panc}$ mice developed pancreata with small areas of normal exocrine pancreas and adipose tissue surrounding sparse islets of Langerhans, suggesting lipomatosis of the exocrine tissue (Supplemental Figure 1, I and J). The remaining exocrine pancreas also had sparse cells showing SA–β-galactosidase activity (Supplemental Figure1K), which is the most accepted biomarker of senescence in vivo (32, 33). Consistent with these findings, low *WASL* expression in human patients correlates with increased expression of the senescence markers *CDKN1A* and *CDKN2A* and the checkpoint kinases *CHK1* and *CHK2* (Figure 1I). Thus, loss of *Wasl* impaired oncogenic *Kras*–driven tumor development by inducing an inflammatory and senescence transcriptional program coupled to a fatty metaplasia.

Concomitant Wasl and Trp53 loss improves survival of Kras-driven tumors and leads to tumors with senescence features. Since the CK-N$^{\Delta Panc}$ mice did not develop tumors, we next analyzed a mouse model with a more aggressive pancreatic tumor. As a model for fast-developing PDAC, we used the *Ptf1a$^{Cre/+}$ Kras$^{LSL\text{-}G12D/+}$ Trp53$^{fl/fl}$* mouse model (34) (hereafter CKP), which has a pancreas-specific homozygous deletion of *Trp53* that results in loss of p53 protein expression (Supplemental Figure 2A) and which develops PDAC within 4–6 weeks in a setting of homozygous *Trp53* deletion. We then assessed the impact of heterozygous and homozygous deletion of *Wasl* in the pancreas of the CKP mouse model. CKP mice lacking 1 *Wasl* allele (hereafter CKP-N^{het}), developed ductal adenocarcinomas, defined by the presence of neoplastic glandular cells in a dense fibrous stroma, and were indistinguishable from CKP mice (Supplemental Figure 2B). Additionally, CKP and CKP-N^{het} mice had a comparable life span (Supplemental Figure 2C). Thus, we used the CKP-N^{het} mice as a control cohort. Homozygous deletion of *Wasl* in CKP mice (hereafter CKP-N$^{\Delta Panc}$) was validated by immunohistochemical staining for N-WASP (Figure 2A), as well as by RT-PCR analysis of *Wasl* expression (Supplemental Figure 2D). The CKP-N$^{\Delta Panc}$ mice had a significantly improved survival compared with CKP-N^{het} mice (Figure 2B), consistent with the improved survival observed in human PDAC patients with low *Wasl*–expressing pancreatic tumors. Similar to the CK-N$^{\Delta Panc}$ mice, the pancreatic tissues of the CKP-N$^{\Delta Panc}$ mice also exhibited high levels of lipomatosis (Figure 2D and Supplemental Figure 2, E and F). We also observed that the CKP-N$^{\Delta Panc}$ tumors were predominantly ductal adenocarcinomas with frequent mesenchymal features (50% of CKP-N$^{\Delta Panc}$ mice, compared with 20% of CKP-N^{het}; Supplemental Table 4), characterized by TWIST- and ZEB1-expressing fibroblasts and macrophages (Supplemental Figure 2, G–I). However, the tumors formed by the CKP-N$^{\Delta Panc}$ mice had a lower proliferation index, as shown by the decreased Ki67 staining (Figure 2C). This suggests that the improved survival seen in the CKP-N$^{\Delta Panc}$ mice is due to delayed tumor development.

Next, we sought to determine the mechanism via which loss of *Wasl* expression in the CKP mice background contributed to improved survival. Oncogenic *Kras* induces cellular senescence, which is suppressed by loss of *Trp53* (27, 33, 35). Accordingly, the lesions in tumors from CK mice were positive for the senescence marker SA–β-galactosidase, and those in CKP tumors were negative (Figure 2E). Notably, deletion of both *Wasl* alleles in the CKP mice background led to the appearance of SA–β-galactosidase–positive

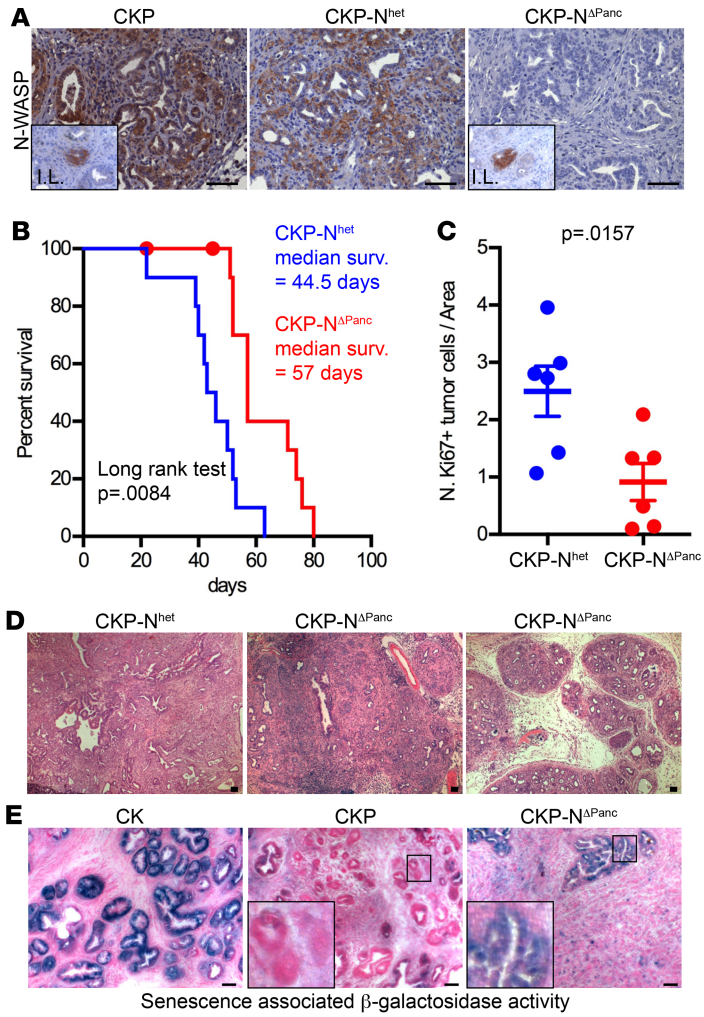

Figure 2. CKP-N$^{\Delta Panc}$ mice have improved survival and develop tumors that express senescent markers. (**A**) Immunohistochemical staining showing the lack of N-WASP expression in pancreata of CKP-N$^{\Delta Panc}$ mice. Scale bars: 50 μM. The inserts show the islets of Langerhans (I.L.) as an internal positive control for N-WASP staining. (**B**) Kaplan-Meier survival curves for mice of the indicated genotypes. CKP-N^{het} (n = 12) and CKP-N$^{\Delta Panc}$ (n = 10). Log-rank test. (**C**) Murine tumor specimen were stained for the proliferation marker Ki67. The number of Ki67-positive tumor cells was quantified per relative area. Data represent mean ± SEM; Student's t test. (**D**) Representative pictures of tumors developed by the indicated mice. Scale bars: 50 μM. (**E**) SA–β-galactosidase staining of cryosections of murine tumors. Scale bars: 50 μM. Inserts show magnification of the black boxes. (**F**) The amount of SA–β-galactosidase–positive cells was quantified in the tumor cell and stromal cell compartment. Data represent the mean of 2 mice per group ± SEM. Student's t test. (**G**) The expression of the indicated genes was analyzed by RT-PCR. Data represent the mean of 4 of 5 tumors per group ± SEM. Student's t test. (**H**) Enrichment plots generated by the GSEA tool. The IL-6/JAK/STAT3 and TNFA signaling via NF-κB signaling pathways, as well as the IFNG response signatures, were enriched in the CKP-N$^{\Delta Panc}$ tumors.

senescent tumor cells (Figures 2, E and F). The CKP-N$^{\Delta Panc}$ tumors also exhibited increased *Cdkn1a(p21)* and *Cdkn2a* expression, along with low *Ccnd1* levels (Figure 2G) and high p16 protein expression (Supplemental Figure 2, J and K). Remarkably, these tumors exhibited a molecular phenotype similar to the tumors of human PDAC patients with low *WASL* expression (compared with Figure 1H). Together, these data indicate that lack of *Wasl* expression overcomes the escape of senescence phenotype observed in the tumors of CKP mice models lacking *Trp53*.

CKP-N$^{\Delta Panc}$ (n = 7) and CKP-N^{het} (n = 6) tumors were next subjected to RNAseq analysis, which identified several differentially expressed genes in the CKP-N$^{\Delta Panc}$ tumors, including *Wips2*/*Ccn5* (Supplemental Table 5) that were validated by RT-PCR analysis (Supplemental Figure 2L). GSEA revealed that the CKP-N$^{\Delta Panc}$ tumors were enriched in genes involved in IL-6 and TNF-α signaling, as well as increased IFN-γ response compared with controls (Figure 2H). Notably these genes are all linked to pathways implicated in a senescence-associated secretory phenotype (SASP) (36).

To investigate if the senescence phenotype observed in CKP-N$^{\Delta Panc}$ tumors is cell autonomous, we used 2 approaches. First, we established cell lines from tumors with different *Wasl* allelic status (CKP, CKP-N^{het}, and CKP-N$^{\Delta Panc}$). Characterization of these cell lines showed a strong SA–β-galactosidase activity in CKP-N$^{\Delta Panc}$ cells only (Figures 3, A and B). Similar to the primary tumors, *Cdkn1a(p21)* expression was increased concomitant with a slightly decreased *Ccnd1* expression (Figure 3C) and low proliferation rates (Supplemental Figure 3A) in CKP-N$^{\Delta Panc}$ cells compared with CKP and CKP-N^{het} cells. Analysis of the culture supernatants using a cytokine profiler revealed increased secretion of some components of the SASP (36), including GM-CSF, KC (CXCL1), and IL-1ra (Figure 3, D and E) in the CKP-N$^{\Delta Panc}$ cells. This is consistent with the lower levels of the SASP-associated genes *GM-CSF* (*CSF2*), *CXCL1*, and *CCL5* (*MCP-2*) (Supplemental Figure 3B) observed in PDAC patients with low *WASL* expression. These data, thus, support a senescent and slow proliferating phenotype of the CKP-N$^{\Delta Panc}$ cells due to lack of *WASL* expression. In the second approach, we isolated tumor organoids (37–39) from both CKP and CKP-N$^{\Delta Panc}$ mouse models. The CKP-N$^{\Delta Panc}$ organoids exhibited delayed growth in 3D-Matrigel cultures (Figure 3F), along with sparse but thicker organoids walls (Figure 3G and Supplemental Figure 3C) and impaired size gain through passaging compared with CKP organoids (Supplemental Figure 3D), indicating the presence of senescent features in the CKP-N$^{\Delta Panc}$ organoids. Altogether, these data demonstrate that lack of *Wasl* delays tumor cell growth and induces senescence in pancreatic tumor cells in a cell-autonomous manner and bypasses the effect of *Trp53* loss.

Loss of Wasl leads to delocalization of N-WASP protein binding partners. Nuclear N-WASP has recently been linked to regulation of senescence (10). However, no nuclear N-WASP staining was observed in CKP and CKP-N^{het} tumors (Figure 2A). Therefore, to understand the mechanism driving the senescence effect of N-WASP loss, we examined its binding partners. N-WASP interacts with WIP and p120ctn through its WH1 and VCA domains, respectively (40, 41). WIP is expressed in all CKP-N^{het} and CKP-N$^{\Delta Panc}$ cancers with comparable protein levels (Supplemental Figure 4A). However, WIP hardly showed a membranous staining pattern in CKP-N$^{\Delta Panc}$ mouse tumors compared with its CKP and CKP-N^{het} counterparts (Figure 4A, Table 1, and Supplemental Figure 4B). In glioblastomas (GB), WIP is involved in the control of the endocytic/endosomal system and in the sequestration of GSK3, which is a component of the β-catenin destruction complex (17). Therefore, we next analyzed the endosomal function of CKP-N$^{\Delta Panc}$ cells and detected increased levels of horseradish peroxidase (HRP) uptake, indicative of increased endocytosis (Figure 4B), along with a GSK3β vesicular staining (Figure 4C). Furthermore, GSK3β staining was weak in CKP-N$^{\Delta Panc}$ tumor tissues compared with CKP-N^{het} control tumor tissues (Supplemental Figure 4C). Based on these findings, we hypothesized that there is endosomal sequestration of destruction complex components in PDAC, akin to GB. We next analyzed the expression of further components of the destruction complex including of phosphorylated β-catenin and YAP1 (42). Phosphorylated β-catenin and YAP1 were enriched in CKP-N$^{\Delta Panc}$ tumors (Figure 4, D, F, and G), while the levels of active (nonphosphorylated) β-catenin and MYC (a β-catenin target gene) were decreased, and there was a downregulation of MYC targets (Figure 4E and Supplemental Figure 4D). We again stratified PDAC patients with high and low *WASL*–expressing tumors using the Xena browser and observed that low *WASL* expression correlated with low expression of the destruction complex components (Figure 4H), consistent with our findings in CKP-N$^{\Delta Panc}$ murine tumors. Thus, our data support a mechanism of endosomal sequestration of the destruction complex components in CKP-N$^{\Delta Panc}$ tumors.

In addition to WIP delocalization, we observed a decrease in the nuclear fraction of p120ctn in CKP-N$^{\Delta Panc}$ tumor cells both by immunofluorescence analysis and Western blot analysis (Figures 5, A–C).

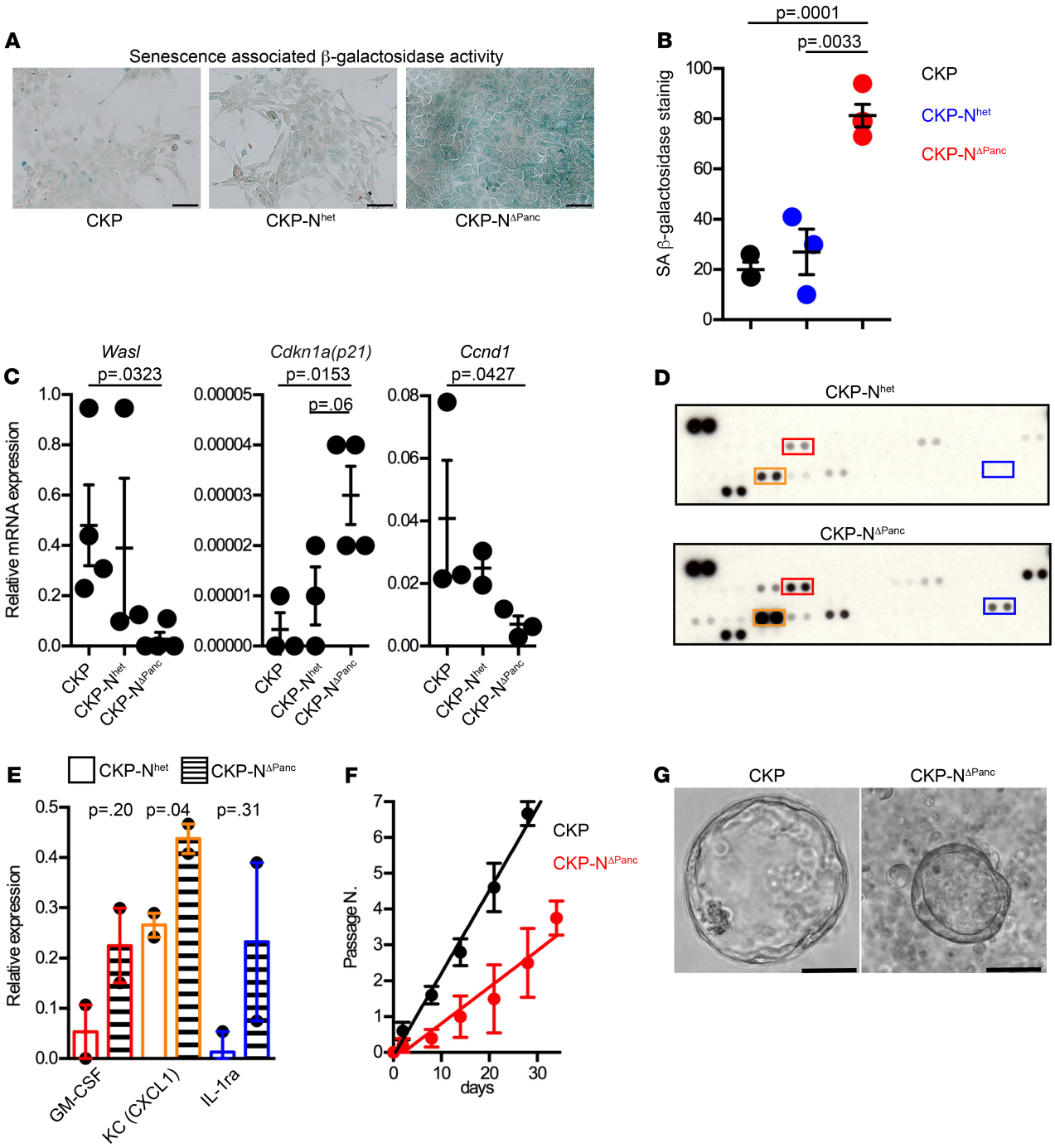

Figure 3. Primary tumor cells isolated from CKP-N$^{\Delta Panc}$ mice have a senescent phenotype. (**A** and **B**) Cell lines from CKP (n = 3), CKP-N^{het} (n = 3), and CKP-N$^{\Delta Panc}$ (n = 4) were grown on a thin layer of collagen and stained for SA–β-galactosidase, quantified in **B**. Data represent mean ± SEM; Kruskal-Wallis 1-way ANOVA test (P = 0.01) followed by Dunn's multiple comparisons test. (**C**) Analysis of gene expression by RT-PCR of primary tumor cell lines isolated from mice of the indicated genotypes (3 of 4 cell lines per group). Data represent mean ± SEM; Kruskal-Wallis 1-way ANOVA test (*Wasl*, P = 0.021; *Cdkn1a*, P = 0.029, *Ccdn1*, P = 0.06) followed by Dunn's multiple comparisons test. (**D**) Conditioned media were collected from CKP-N^{het} and CKP-N$^{\Delta Panc}$ cells, which were grown on a thin layer of collagen for cytokine array analysis. The boxed regions on the representative blot indicate the differentially secreted cytokines. (**E**) Quantification of the boxed regions as described in **D**. Data represent the mean of 2 cell lines per group ± SEM. Student's t test. (**F** and **G**) Organoids generated from CKP (n = 5) and CKP-N$^{\Delta Panc}$ (n = 5) pancreata were isolated. The passage numbers in function of the time are shown. Data represent mean ± SEM. (**F**) Organoids generated from CKP (n = 5) and CKP-N$^{\Delta Panc}$ (n = 5) pancreata were cultivated. The passage numbers in function of the time are shown. Data represent mean ± SEM. The slopes are substantially different indicating a slower growth of the CKP-N$^{\Delta Panc}$ organoids. (**G**) Representative bright-field images of organoids 14 days after isolation. The CKP-N$^{\Delta Panc}$ organoids were not passaged during this period, while the CKP organoids were passaged 3 times.

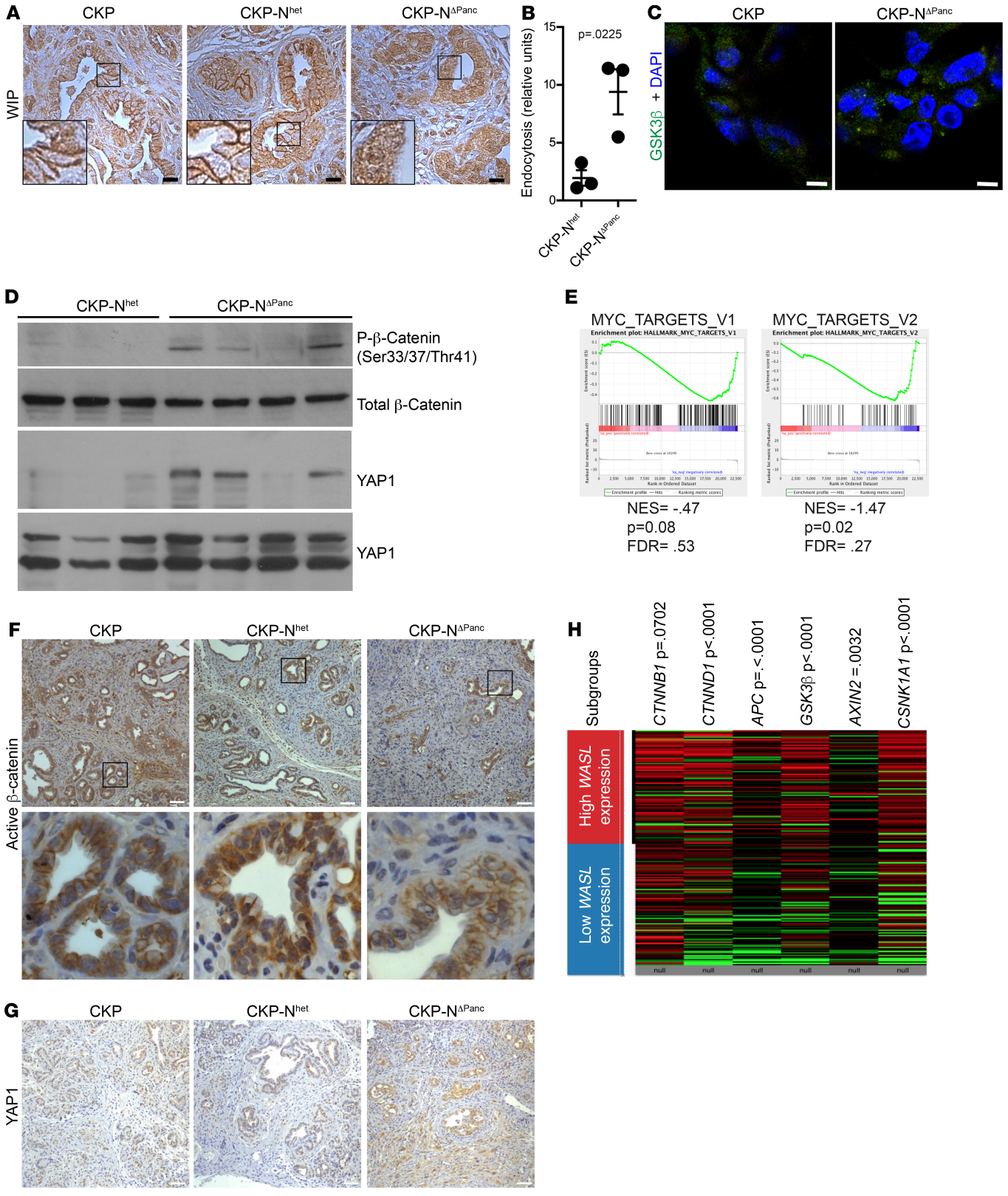

Figure 4. Lack of *Wasl* leads to the accumulation of components of the destruction complex and increased expression of inactive β-catenin. (**A**) Immunohistochemical staining for WIP in murine tumors. Scale bars: 50 M. Inserts show magnification of the black boxes. (**B**) Three cell lines per genotype were grown overnight; then, an HRP-endocytic assay was performed. The relative endocytosis level is shown. Each point represents the mean from 3 experiments, and the mean of 3 cell lines ± SEM is shown. Student's *t* test. (**C**) Cells were grown on a thin layer of collagen, and an immunofluorescence staining for GSK3β was performed. Nuclei are counterstained with DAPI. Scale bars: 10 μM. (**D**) Western blot analysis showing β-catenin phosphorylation at Ser33/37 and Thr41, as well as total YAP1. Actin and ERK1 + ERK2 were used as loading controls. (**E**) Enrichment plots

generated by the GSEA tool. The signatures for MYC targets were enriched in the CKP-N$^{\Delta Panc}$ tumors. (**F** and **G**) Immunohistochemical stainings for active β-catenin and YAP1. Scale bars: 50 M. The right panels show magnification of the black boxes. (**H**) PDAC patients were stratified for *WASL* expression using the UCSC Xena genomic browser, and the expression levels of the indicated genes were compared. *WASL* high (n = 86), *WASL* low (n = 89). Unpaired t test with Welch's correction.

Nuclear p120ctn has been shown to interact with, and regulates the transcriptional activity of, the multifaceted transcription factor KAISO (encoded by the *Zbtb33* gene) that negatively regulates Wnt/β-catenin signaling (43–46). Therefore, we examined KAISO expression in CKP-N$^{\Delta Panc}$ tumor cells. Notably, we detected increased KAISO protein expression in CKP-N$^{\Delta Panc}$ tumors (Figure 5, D and E), as well as in the matched isolated cells, compared with controls (Supplemental Figure 5, A and B). However, there was no apparent increase in *Kaiso* gene expression (Supplemental Figure 5C), suggesting that Kaiso is posttranslationally regulated and/or stabilized in CKP-N$^{\Delta Panc}$ tumors. In addition, we detected less colocalization of KAISO with the active transcription marker H3K4 in CKP-N$^{\Delta Panc}$ tumor cells compared with controls (Supplemental Figure 5, D and E), suggesting a displacement of KAISO from active promoter regions (47–49). We next assessed the endogenous p120ctn/KAISO interaction using immunoprecipitation assays and detected the p120ctn/KAISO complex in CKP-N$^{\Delta Panc}$ tumor cells (Supplemental Figure 5F).

In summary, lack of N-WASP in CKP tumors correlates with an enrichment of endocytosis concomitant with an accumulation of components of the β-catenin destruction complex and the transcription factor KAISO but with nuclear displacement of Kaiso's binding partner p120ctn.

Inhibition of endocytosis and increased nuclear p120ctn are required to rescue the phenotype of CKP-N$^{\Delta Panc}$ tumor cells. To confirm the involvement of the destruction complex and p120ctn in the phenotype of the CKP-N$^{\Delta Panc}$ tumors, we performed the following functional experiments. First, we treated CKP-N$^{\Delta Panc}$ tumor cells with endocytosis inhibitors. We included Cytochalasin D (which inhibits actin polymerization), the Na^+/H^+ exchanger ethyl-isopropyl-amiloride (EIPA), and the ionophore salinomycin. All treatments strongly induced cytoplasmic GSK3β localization concomitant with decreased total YAP1 protein expression (Figure 6, A and B). This result indicates the successful inhibition of the GSK3β endosomal sequestration. The 24-hour EIPA treatment downregulated *Ccnd1* expression in the control cell lines, consistent with published studies (50) (data not shown). All treatments slightly upregulated *Cdkn1a(p21)* (Figure 6C) and downregulated *Ccnd1* (Supplemental Figure 6A) but had no significant effect on the number of senescent cells (Figure 6D). Therefore, this treatment — although inducing a decrease of YAP1 in the CKP-N$^{\Delta Panc}$ tumor cells — was not able to rescue their senescence phenotype. Next, based on the observation of decreased nuclear p120ctn in CKP-N$^{\Delta Panc}$ tumors cells, we treated CKP-N$^{\Delta Panc}$ tumor cells with leptomycin B (LMB) since p120ctn nucleocytoplasmic shuttling is sensitive to LMB treatment (Figure 6E) (43, 51). However, LMB treatment alone was not sufficient to rescue the senescence phenotype of CKP-N$^{\Delta Panc}$ tumor cells (Supplemental Figure 6). We next treated CKP-N$^{\Delta Panc}$ tumor cells with a combination of salinomycin and LMB, which target both deregulated pathways in the CKP-N$^{\Delta Panc}$ tumor cells. This sequential treatment of CKP-N$^{\Delta Panc}$ tumor cells rescued the senescent phenotype of CKP-N$^{\Delta Panc}$ tumor cells, as shown by the significant decrease of senescence-associated β-galactosidase activity (Figures 6, F and G) and downregulation of *Cdkn1a(p21)* in the CKP-N$^{\Delta Panc}$ tumor cells (Figure 6H). Collectively, our data confirm that *Wasl* loss regulates pancreatic tumor cell senescence by both inducing the endosomal sequestration of the β-catenin destruction complex components GSK3β and YAP1 and by inducing mislocalization of p120ctn.

This study shows that N-WASP acts as an oncogene in the development of PDAC by regulating protein stability and subcellular localization of components of the p120ctn/β-catenin signaling pathway.

Discussion

Kras^{G12D} is the driver oncogenic mutation of PDAC (1). However, despite extensive research, the precise molecular mechanism involved in PDAC development and progression is not well understood. The effectors of oncogenic *Kras* include CDC42 and PIP2, both binding partners of N-WASP (encoded by *Wasl*) (12–14, 52), which is associated with poor PDAC prognosis (7). Originally, N-WASP was investigated in the pathogenesis of the human Wiskott-Aldrich syndrome, where it regulates immunity by interacting with histone methyltransferases (53). At a molecular level, N-WASP acts as an actin nucleation-factor (54); thus, it is not surprising that it is implicated in the regulation of cell migration and tumor metastasis (7–9, 11). More recently, nuclear N-WASP was reported as an inhibitor of p53-induced senescence in a model for skin tumor formation, further implicating an oncogenic role for N-WASP (10). However,

Table 1. Morphometric quantification of WIP staining

WIP staining	Cytoplasmic			Membranous		Nuclear	Stroma
Genotype	–	+	++	–	+		
CKP-N$^{\Delta Panc}$	4/12	7/12	1/12	9/10	1/10	4/12	12/12
CKP-N^{het}	4/8	2/8	2/8	1/8	7/8	8/8	3/8
CKP	0/4	3/4	1/4	0/4	4/4	4/4	3/4

Morphometric quantification of the WIP staining described in Figure 4A. Representative pictures for absent (–), weak (+), or strong (++) cytoplasmic staining; membranous and nuclear or stromal staining are shown in Supplemental Figure 4B. The assessment of the staining was done in a blinded fashion.

N-WASP has also been shown to act as a tumor suppressor, for example, in early intestinal carcinogenesis, suggesting a tissue-specific function of this protein (55). Since N-WASP binds KRAS effectors and because actin polymerization is one of the pathways involved in PDAC development (15), we hypothesized that *Wasl* expression plays a tumor-promoting role in PDAC development.

Using established oncogenic *Kras*–based mouse models for PDAC, we show that the conditional deletion of *Wasl* delays PDAC development, leading to senescent tumors in the absence of the tumor suppressor *Trp53*, and abrogates tumor development in the CK mouse model, highlighting the oncogenic properties of *Wasl* in PDAC. In both mouse models, we observed increased lipomatosis, and RNAseq showed that *Wisp2*/*Ccn5* was among the significantly upregulated genes upon loss of *Wasl*. *Wisp2* encodes a cytoplasmic protein downregulated in PDAC, which is involved in the suppression of cell proliferation, reviewed in ref. 56; *Wisp2* also regulates adipogenic commitment (57). Both known functions of *Wisp2* are consistent with the low proliferation rate and the increased fatty metaplasia observed after deletion of *Wasl* in the CKP

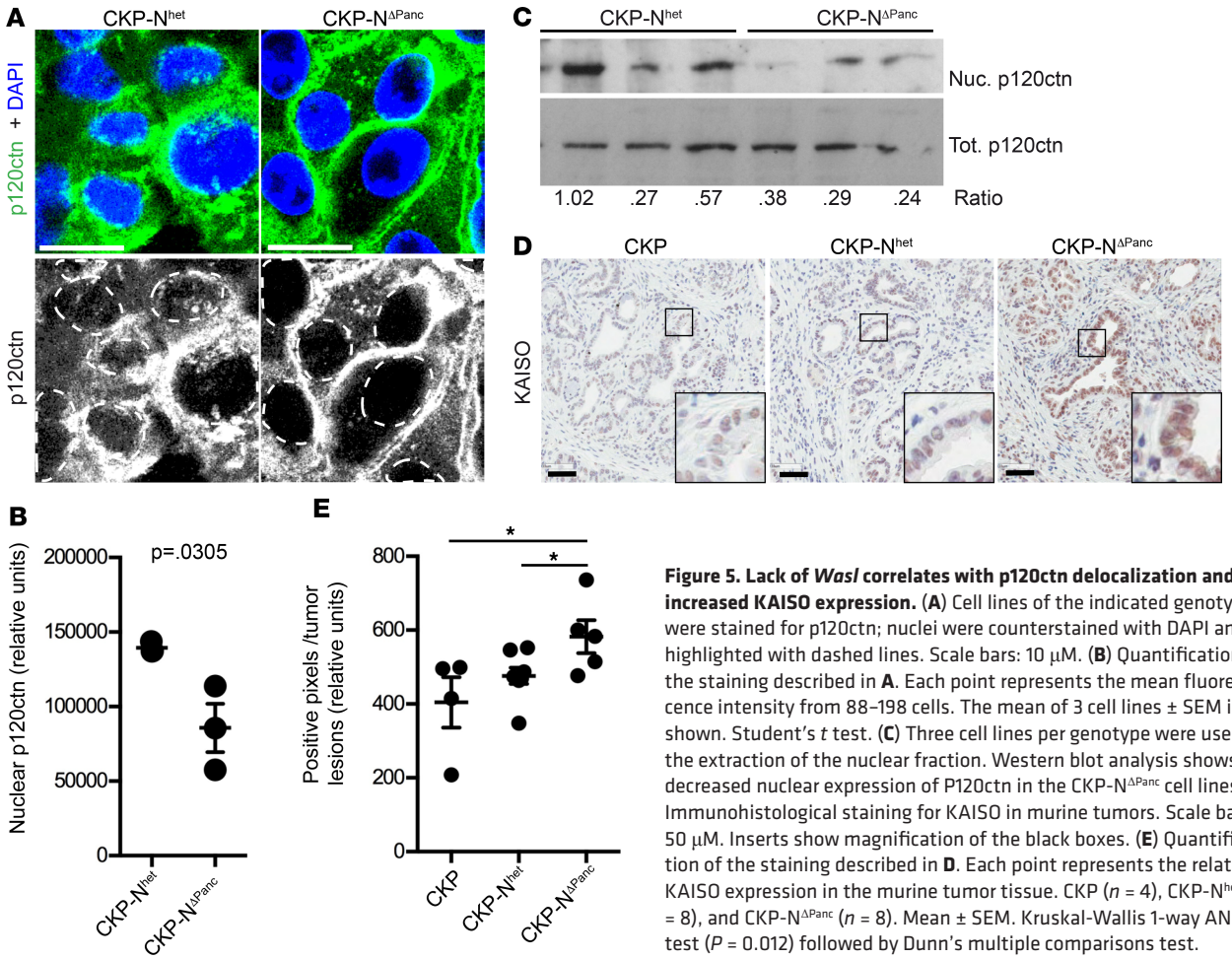

Figure 5. Lack of *Wasl* correlates with p120ctn delocalization and with increased KAISO expression. (**A**) Cell lines of the indicated genotype were stained for p120ctn; nuclei were counterstained with DAPI and are highlighted with dashed lines. Scale bars: 10 μM. (**B**) Quantification of the staining described in **A**. Each point represents the mean fluorescence intensity from 88–198 cells. The mean of 3 cell lines ± SEM is shown. Student's *t* test. (**C**) Three cell lines per genotype were used for the extraction of the nuclear fraction. Western blot analysis shows a decreased nuclear expression of P120ctn in the CKP-N$^{\Delta Panc}$ cell lines. (**D**) Immunohistological staining for KAISO in murine tumors. Scale bars: 50 μM. Inserts show magnification of the black boxes. (**E**) Quantification of the staining described in **D**. Each point represents the relative KAISO expression in the murine tumor tissue. CKP (n = 4), CKP-N^{het} (n = 8), and CKP-N$^{\Delta Panc}$ (n = 8). Mean ± SEM. Kruskal-Wallis 1-way ANOVA test (P = 0.012) followed by Dunn's multiple comparisons test.

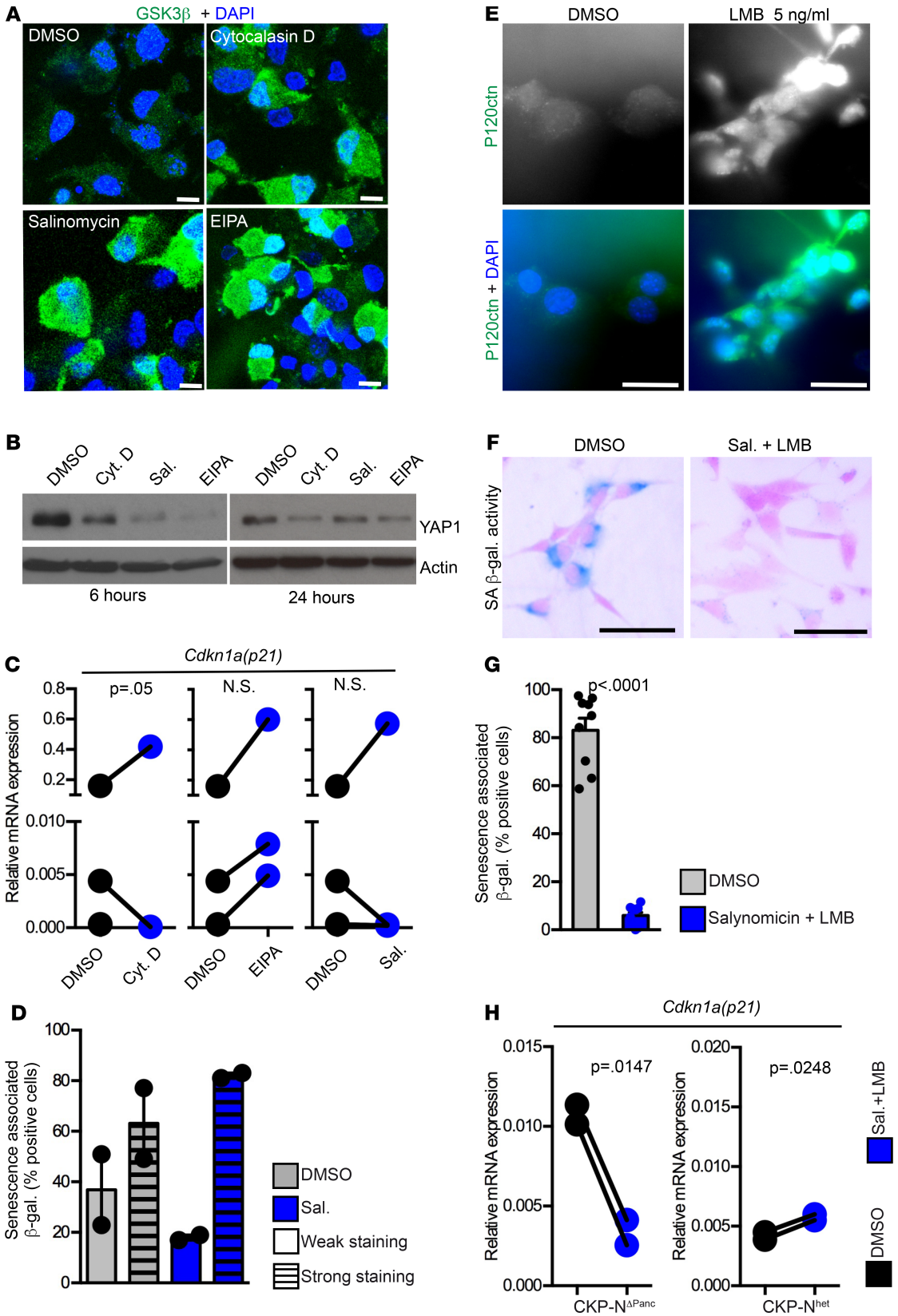

Figure 6. Combined salinomycin and LMB treatment of CKP-N$^{\Delta Panc}$ tumor cells rescues the senescent phenotype. (**A**) CKP-N$^{\Delta Panc}$ cells were treated with Cytochalasin D (2 μM), salinomycin (1 μM), or EIPA (25 μM) for 48 hours; then, the cells were fixed and stained for GSK3β. Scale bars: 10 μM. (**B**) CKP-N$^{\Delta Panc}$ cells were treated as described for **A**, harvested, and analyzed by Western blot. (**C**) Three CKP-N$^{\Delta Panc}$ cell lines were treated as described for **A** for 24 hours and harvested, and the relative *Cdkn1a(p21)* expression was analyzed by RT-PCR. Student's *t* test. (**D**) CKP-N$^{\Delta Panc}$ cells were grown on a thin layer of collagen and treated with salinomycin; then, the cells fixed stained for SA–β-galactosidase and quantified. The mean of 2 cell lines ± SEM is shown. Student's *t* test.

(**E**) CKP-N$^{\Delta Panc}$ cells were treated with LMB (5 ng/mL) for 20 hours; then, the cells were fixed and stained for p120ctn. Scale bars: 50 μM. (**F**) CKP-N$^{\Delta Panc}$ cells were grown on a thin layer of collagen and sequentially treated with 1M salinomycin and 5 ng/mL LMB; then, the cells fixed stained for SA–β-galactosidase. A representative image is shown. Scale bars: 50 μM. **(G)** Quantification of the treatment described in **F**; each treatment was performed in triplicates. The mean of 3 cell lines ± SEM is shown. Student's *t* test. (**H**) Cell lines were treated as described for panel F. The relative *Cdkn1a(p21)* expression of 2 cell lines is shown. Student's *t* test.

mouse model. Notably, *Wisp2* was slightly upregulated in 4-week-old CK-N$^{\Delta Panc}$ mice, supporting an early function of *Wisp2* upon loss of *Wasl*.

PDAC patients stratified for low *WASL* expression have improved survival and exhibit low expression of senescence markers, as well as downregulation of the Wnt/β-catenin pathway; thus, mechanistically, we focused on the tumors developed by the CKP-N$^{\Delta Panc}$ mice, which showed similar molecular features to low *WASL*–expressing human PDAC tumor tissues rather than investigating the CK-N$^{\Delta Panc}$ mice, which do not develop tumors.

CKP-N$^{\Delta Panc}$ mice developed slightly more mesenchymal tumors than control mice. This phenotype can be explained by the combined action of several factors, as described below. First, we observed high Kaiso expression in CKP-N$^{\Delta Panc}$ tumors. Since Kaiso is implicated in regulation of the mesenchymal phenotype and high Kaiso expression correlates with poor survival of many different tumor types (prostate, breast, pancreas; reviewed in ref. 48), this raises the possibility that Kaiso plays a role in *Wasl*-driven PDAC. Second, the CKP-N$^{\Delta Panc}$ tumors have increased YAP1 expression, which is also involved in regulating the mesenchymal phenotype (58). Last but not least, our detection of increased inflammation (which is intimately connected to induction of epithelial-mesenchymal transition EMT; ref. 59) in CKP-N$^{\Delta Panc}$ and CK-N$^{\Delta Panc}$ mice further supports a *Wasl* mechanism involving EMT. Interestingly, although EMT is linked to worse PDAC survival outcomes (60), our CKP-N$^{\Delta Panc}$ mice did not exhibit poor survival, most likely because there was no tumor metastasis. However, the improved survival of CKP-N$^{\Delta Panc}$ mice may also be explained by the low proliferating senescent tumors. We showed that loss of *Wasl* led to a cell-autonomous senescent phenotype in the tumors, consistent with strong upregulation of *Cdkn1a(p21)* and increased SA–β-galactosidase activity that is currently the most accepted biomarker of senescence in vivo (32, 33). Cellular senescence has been described as a tumor-suppressive mechanism (36). However, senescent cells can modify the tumor microenvironment by acquisition of SASP, which can increase the number of inflammatory cells (36, 61), as evidenced by the GSEA signature for an inflammatory response in the CKP-N$^{\Delta Panc}$ tumors.

Since no nuclear N-WASP was detected in CKP-N$^{\Delta Panc}$ tumors, we focused on N-WASP interacting proteins (WIP and p120ctn) rather than on the deregulated genes (12, 13). N-WASP interacts with the actin cytoskeleton, which in turn regulates cell motility and is not linked to senescence (12, 13). N-WASP additionally binds WIP and p120ctn. WIP is required for N-WASP and YAP1 stabilization by sequestration of the β-catenin destruction complex (12, 17, 40). YAP1 is involved in several signaling pathways, where it plays a different role depending on the upstream members (62). WIP is also involved in the regulation of endocytosis (63) and participates in several cellular processes, some of which are relevant in cancer and which may be dependent on different oncogenic stimuli (17, 64, 65). We showed that CKP-N$^{\Delta Panc}$ tumors displayed a small amount of membranous WIP, which probably resulted in the increased rate of endocytosis that we observed in these tumors. In line with the role of WIP in the sequestration of destruction complex components, we observed vesicular staining of GSK3β, as well as high YAP1 and phosphorylated β-catenin levels. Since inhibition of endocytosis induced cytosolic accumulation of GSK3β and decrease of YAP1 expression, we conclude that loss of N-WASP in our mouse model leads to sequestration of the destruction complex into vesicles. We recently showed that *Wasl* deletion impairs ADM by inhibiting fluid-phase endocytosis in pancreatic acinar cells (6). Juin and colleagues created a conditional mouse model with a mosaic deletion of *Wasl* and concomitant activation of oncogenic *Kras* and mutated p53 (*Trp53*^{R172H}) (KPCN mice) (9). In this KPCN model, *Wasl* loss deregulated vesicular transport, reduced metastasis, and improved survival. These 2 studies in conjunction with our current study reveal a crucial role for N-WASP in PDAC development through regulation of vesicular trafficking.

The second N-WASP binding partner that we focused on is p120ctn. CKP-N$^{\Delta Panc}$ tumors had less nuclear p120ctn, which is consistent with better prognosis of PDAC patients (18). p120ctn is also involved in the internalization of the GSK3β-containing destruction complex into multivesicular bodies (66); thus, the delocalization p120ctn upon loss of *Wasl* likely affected the vesicular sequestration of destruction complex components. P120ctn shuttles to and from the nucleus, where it interacts with the transcription factor

Kaiso, which is upregulated in CKP-N$^{\Delta Panc}$ tumors (43–45, 48, 67). Since we detected low p120ctn nuclear levels in the CKP-N$^{\Delta Panc}$ tumor cells, we reasoned that p120ctn undergoes increased nucleocytoplasmic shuttling in our model. We were, however, only able to rescue the senescence-associated phenotype in CKP-N$^{\Delta Panc}$ tumor cells by inducing nuclear p120ctn translocation along with inhibition of endocytosis. In summary, our study implicates p120ctn nucleocytoplasmic shuttling and accumulation of destruction complex components in the senescence phenotype of CKP-N$^{\Delta Panc}$ tumor cells and, by extension, suggest a role for N-WASP in these processes in PDAC tumor development.

Notably, lack of *Wasl* — in the context of oncogenic *Kras* only — led to an inflammatory phenotype at an early time point. Pancreatitis is considered an important factor that promotes both human and murine PDAC (2, 30, 31). However, despite the inflammatory phenotype at 4 weeks of age, which completely regressed within 6 months, the CK-N$^{\Delta Panc}$ mice did not develop tumors. Since injury of acinar cells can lead to fatty degeneration in pancreatitis (60), this is consistent with the CK-N$^{\Delta Panc}$ phenotype at endpoint. Similar to the CKP-N$^{\Delta Panc}$ mouse model, GSEA in CK-N$^{\Delta Panc}$ mice showed an increased IL-6 signaling signature, along with an INFG response. Thus, the CK-N$^{\Delta Panc}$ phenotype resembles some senescence features of the CKP-N$^{\Delta Panc}$ mouse model. These findings are of potential interest to elucidate the role of inflammation in PDAC development and may be investigated in further studies.

In conclusion, *Wasl* is required for the suppression of *Kras*-induced senescence upon *Trp53* loss (27, 35). Given the importance of senescence in PDAC (27), unraveling a connection between N-WASP, senescence, and the p120ctn/β-catenin pathway may provide strategies for the treatment of pancreatic cancer.

Methods

Mice. *Ptf1a*$^{Cre/wt}$, *Kras*$^{LSL\text{-}G12D/wt}$, *Trp53*$^{fl/fl}$, and *Wasl*$^{fl/fl}$ strains have previously been described (6, 9, 20, 34, 68, 69).

IHC and immunofluorescence staining. The primary antibodies used are listed in Supplemental Table 6. Immunoperoxidase staining was performed on 4% PFA/PBS fixed paraffin-embedded tissue slides using the Vectastain-ABC-Elite and/or the ImmPRESS kit (Vector Laboratories) following manufacturer's instructions. For immunofluorescence staining, samples were fixed with 2% PFA for 10 minutes and permeabilized with 0.1% Triton X-100 for 5 minutes. Slides were incubated overnight with primary antibodies (listed in Supplemental Table 6) at 4°C and were then incubated for 1 hour with secondary antibodies (Alexa dyes, 1:500, Invitrogen) at room temperature. Coverslips were mounted on tissue sections with VECTASHIELD HardSet Mounting Medium containing DAPI (Vector Laboratories) and examined using a Leica TCS_SP5 confocal microscope. In all experiments, samples were stained sequentially. To avoid bleed-through, single channels were scanned sequentially. Primary antibodies used are listed in the Supplemental Table 6.

Morphometric analysis. Slides from murine tissue were digitalized, and the regions of interest were quantified blindly using Aperio-ImageScope from Leica. Alternatively, several randomly chosen pictures were taken using a 10× objective from the stained slides, and positive staining was quantified blindly by different researchers.

Cell culture. Primary pancreatic tumor cells were derived from transgenic mouse tumors described above and maintained in DMEM media (Sigma-Aldrich, catalog D0819) supplemented with 10% FCS (Thermo Fisher Scientific). Cells were incubated in a humidified incubator at 37°C and 5% CO_2. Where specified, the cell culture dishes were coated with a thin layer of collagen using rat tail collagen type I (Corning) according the manufacturer's instructions. For inhibition of endocytosis, the following inhibitors were used: salinomycin (MilliporeSigma, S6201), Cytochalasin D (Tocris, 1233/1), and EIPA (Tocris, 3378/10). LMB was purchased from Sigma-Aldrich.

Organoid isolation and maintenance. Tumor cells were isolated and cultured as previously described (19, 37, 38, 70, 71). Briefly, after euthanizing the mice, the pancreas was quickly harvested and washed in PBS plus penicillin-streptomycin. The pancreas was then minced into small pieces and further digested with collagenase type IV (Sigma-Aldrich) for 1 hour. Additional digestion with Trypsin for 5 to 10 minutes was performed. Pancreatic cells were further washed and centrifuged at 200 × *g* for 5 minutes at 4 °C. The cells were mixed with Matrigel, and the mixture was plated (50 μL per well of a 24-well plate) and allowed to solidify. After 20 minutes, when the Matrigel had solidified, complete culture media (37) was added to cells.

Immunoprecipitation and Western blots. Immunoprecipitation and Western blot analyses were performed as previously described (6, 44). Primary antibodies used are listed in Supplemental Table 6. Antibody binding was visualized using HRP–labeled secondary antibodies (1:10,000) (GE Healthcare, catalog NA935V, NA394V, and NA931V) and ECL reagent (GE Healthcare).

Quantitative PCR. Total RNA extraction was performed according to manufacturer's instructions using QIAGEN RNeasy Plus Micro Kit (catalog 74034) for organoids and the NucleoSpin RNA kit (Machery-Nagel) for all other samples. RNA was reverse transcribed to cDNA using Super ScriptIII reverse transcriptase and oligo(dT) primers (Thermo Fisher Scientific) following manufacturer's instructions. The resultant cDNA was used as template for quantitative PCR (qPCR). RT-PCR was performed in duplicates, using the iTaq universal SYBR Green (Bio-Rad) according to manufacturer's instructions. Primers used are listed in Supplemental Table 7. The relative amount of each gene of interest was normalized to the housekeeping gene XS13 (an acidic ribosomal protein, which is constitutively expressed at the same level in normal, cancerous, and inflamed pancreas; ref. 24) using the ΔΔCT method.

RNAseq and GSEA by Enrichr. RNA extraction was performed as described for qPCR. RNA concentration was fluorimetrically determined using the QuBit 3.0 system (Thermo Fisher Scientific). Bulk 3′-prime transcript end RNAseq (SCRB-Seq) libraries were prepared as described below. RNA was reverse transcribed using oligo(dT) primers decorated with sample barcodes, unique molecular identifiers (UMIs), and adapters (Integrated DNA Technologies). cDNA from all samples was pooled, and unincorporated primers were digested using Exonuclease I (New England Biolabs). The cDNA pool was then amplified with KAPA HiFi ReadyMix (KAPA Biosystems). To obtain sequencing libraries, 0.8 ng of cDNA was fragmented, and 3′ ends were amplified with the Nextera XT Kit (Illumina) using a specific primer for the adapter on the 3′-end. The library was paired-end sequenced on a HiSeq1500 with 16 cycles for read 1 to decode sample barcodes and UMIs, and 51 cycles on read 2 into the cDNA fragment. Transcript and gene definitions were used according to the ENSEMBL annotation release 75. GSEA was performed using the web tool Enrichr, available at http://amp.pharm.mssm.edu/Enrichr (23, 24). In addition, GSEA Software v4.0.3 (72) was used to calculate normalized enrichment scores (NES), false discovery rate (FDR) values, and *P* values for gene sets in the Molecular signatures database (MSigDB) (73). The genes were preranked according to the fold-change and *P* values

Endocytosis assay. A fluid-phase HRP uptake assay was used as described previously (6). Briefly, samples were incubated with 1 mg/mL HRP (MilliporeSigma) for 5 minutes. After pulse, chase, and extensive wash, cells were lysed (10 mM TRIS, 0.05% Triton X-100). The amount of internalized HRP was quantified by measuring the peroxidation of o-Dianisidine (MilliporeSigma) after addition of H_2O_2 at 405 nm. The amount of internalized HRP was normalized to the total protein content measured by BCA protein assay (Pierce).

SA–β-galactosidase staining. SA–β-galactosidase staining was performed as previously described (33). Briefly, the fixed samples were incubated with a staining solution containing 20 mg/mL of X-Galactosidase (Roth) for 1–3 days at 37°C and then mounted. Stained cells were examined with a Zeiss inverse microscope, and images were quantified blindly with ImageJ (NIH).

In silico patient survival. For stratification of PDAC patients, we used the UCSC Xena Platform (http://xena.ucsc.edu) (74) with the TCGA Pancreatic Cancer (PAAD) data set filtered for primary tumors ($n = 185$).

Statistics. Statistical analyses were performed using the GraphPad Prism version 5.0a for Mac OS X. We applied unpaired, 2-tailed Student's *t* test, Mann-Whitney *U* test, the 2-way ANOVA, and the log-rank test; for multiple comparisons, we used the Kruskal-Wallis test followed by a Dunn's multiple comparisons test, as specified in the legends. A *P* value less than 0.05 was considered significant.

Study approval. The present study in animals was reviewed and approved by the Government of Bavaria, Munich, Germany (AZ 5.2-1-54-2532-46-2014) and the IACUC of the Technical University of Munich. Experiments were conducted in accordance with the German Federal Animal Protection Laws.

Author contributions

AHS, ZD, JD, and K. Schulte performed and analyzed experiments. CLM designed experiments, analyzed data, and wrote the manuscript. AHS, ZD, JD, HE, RMS, and CLM discussed the manuscript. HKE, BBA, LR, JMD, and K. Steiger performed tissue staining and molecular analyses. ASAA performed experiment for the revision. ML planned and discussed senescence experiments. AHS, ZD, JD, BBA, LR, JMD, ML, ASAA, and MR edited the manuscript. RO, TE, and RR were in involved in RNAseq experiments and analysis. HE performed GSEA analyses MR, GVF, JTS, RMS, and CLM provided funding.

Acknowledgments

We would like to thank D. Tuveson and C. Brakebusch for providing transgenic animals. We thank B.K. Bhatti for technical help. The results published here are, in part, based upon data generated by using the UCSC Xena Platform for cancer genomics data visualization and interpretation (http://xena.ucsc.edu). This project was supported by the Deutsche Forschungsgemeinschaft (LU1943/1 and LU1943/1-2, to CLM; SI1549/2-1 and SI1549/3-1 (KFO337), to JTS), the SFB1321 Modeling and Targeting Pancreatic Cancer (to RR, MR, GVF and RMS), the SFB824 (project C4 to JTS), and the German Cancer Aid Foundation (Deutsche Krebshilfe 111273 to MR and 70112505 to JTS).

Address correspondence to: Clara Lubeseder-Martellato, Klinikum rechts der Isar Technical University of Munich, Klinik und Poliklinik für Innere Medizin II, Ismaninger Strasse 22 81675 München, Germany. Phone: 49.0.89.4140.6792; Email: clara.lubeseder-martellato@tum.de.

1. Almoguera C, Shibata D, Forrester K, Martin J, Arnheim N, Perucho M. Most human carcinomas of the exocrine pancreas contain mutant c-K-ras genes. *Cell*. 1988;53(4):549–554.
2. Bardeesy N, DePinho RA. Pancreatic cancer biology and genetics. *Nat Rev Cancer*. 2002;2(12):897–909.
3. Aichler M, et al. Origin of pancreatic ductal adenocarcinoma from atypical flat lesions: a comparative study in transgenic mice and human tissues. *J Pathol*. 2012;226(5):723–734.
4. Kopp JL, et al. Identification of Sox9-dependent acinar-to-ductal reprogramming as the principal mechanism for initiation of pancreatic ductal adenocarcinoma. *Cancer Cell*. 2012;22(6):737–750.
5. Means AL, et al. Pancreatic epithelial plasticity mediated by acinar cell transdifferentiation and generation of nestin-positive intermediates. *Development*. 2005;132(16):3767–3776.
6. Lubeseder-Martellato C, et al. Oncogenic KRas-induced Increase in Fluid-phase Endocytosis is Dependent on N-WASP and is Required for the Formation of Pancreatic Preneoplastic Lesions. *EBioMedicine*. 2017;15:90–99.
7. Guo JC, et al. N-wasp in pancreatic ductal adenocarcinoma: associations with perineural invasion and poor prognosis. *World J Surg*. 2014;38(8):2126–2131.
8. Hou J, et al. N-WASP promotes invasion and migration of cervical cancer cells through regulating p38 MAPKs signaling pathway. *Am J Transl Res*. 2017;9(2):403–415.
9. Juin A, et al. N-WASP Control of LPAR1 Trafficking Establishes Response to Self-Generated LPA Gradients to Promote Pancreatic Cancer Cell Metastasis. *Dev Cell*. 2019;51(4):431–445.e7.
10. Li H, Petersen S, Garcia Mariscal A, Brakebusch C. Negative Regulation of p53-Induced Senescence by N-WASP Is Crucial for DMBA/TPA-Induced Skin Tumor Formation. *Cancer Res*. 2019;79(9):2167–2181.
11. Martin TA, Pereira G, Watkins G, Mansel RE, Jiang WG. N-WASP is a putative tumour suppressor in breast cancer cells, in vitro and in vivo, and is associated with clinical outcome in patients with breast cancer. *Clin Exp Metastasis*. 2008;25(2):97–108.
12. Alekhina O, Burstein E, Billadeau DD. Cellular functions of WASP family proteins at a glance. *J Cell Sci*. 2017;130(14):2235–2241.
13. Rohatgi R, Ho HY, Kirschner MW. Mechanism of N-WASP activation by CDC42 and phosphatidylinositol 4, 5-bisphosphate. *J Cell Biol*. 2000;150(6):1299–1310.
14. Eser S, Schnieke A, Schneider G, Saur D. Oncogenic KRAS signalling in pancreatic cancer. *Br J Cancer*. 2014;111(5):817–822.
15. Heid I, et al. Early requirement of Rac1 in a mouse model of pancreatic cancer. *Gastroenterology*. 2011;141(2):719–730.
16. Zhang W, et al. Downstream of mutant KRAS, the transcription regulator YAP is essential for neoplastic progression to pancreatic ductal adenocarcinoma. *Sci Signal*. 2014;7(324):ra42.
17. Gargini R, Escoll M, García E, García-Escudero R, Wandosell F, Antón IM. WIP Drives Tumor Progression through YAP/TAZ-Dependent Autonomous Cell Growth. *Cell Rep*. 2016;17(8):1962–1977.
18. Mayerle J, et al. Up-regulation, nuclear import, and tumor growth stimulation of the adhesion protein p120 in pancreatic cancer. *Gastroenterology*. 2003;124(4):949–960.
19. Reichert M, Takano S, Heeg S, Bakir B, Botta GP, Rustgi AK. Isolation, culture and genetic manipulation of mouse pancreatic ductal cells. *Nat Protoc*. 2013;8(7):1354–1365.
20. Hingorani SR, et al. Preinvasive and invasive ductal pancreatic cancer and its early detection in the mouse. *Cancer Cell*. 2003;4(6):437–450.
21. Li Q, et al. Reg proteins promote acinar-to-ductal metaplasia and act as novel diagnostic and prognostic markers in pancreatic ductal adenocarcinoma. *Oncotarget*. 2016;7(47):77838–77853.
22. Morris JP, Cano DA, Sekine S, Wang SC, Hebrok M. Beta-catenin blocks Kras-dependent reprogramming of acini into pancreatic cancer precursor lesions in mice. *J Clin Invest*. 2010;120(2):508–520.
23. Chen EY, et al. Enrichr: interactive and collaborative HTML5 gene list enrichment analysis tool. *BMC Bioinformatics*. 2013;14:128.
24. Kuleshov MV, et al. Enrichr: a comprehensive gene set enrichment analysis web server 2016 update. *Nucleic Acids Res*. 2016;44(W1):W90–W97.
25. Wan MH, et al. Review of experimental animal models of biliary acute pancreatitis and recent advances in basic research. *HPB (Oxford)*. 2012;14(2):73–81.
26. Kuilman T, et al. Oncogene-induced senescence relayed by an interleukin-dependent inflammatory network. *Cell*. 2008;133(6):1019–1031.
27. Porciuncula A, Hajdu C, David G. The Dual Role of Senescence in Pancreatic Ductal Adenocarcinoma. *Adv Cancer Res*. 2016;131:1–20.

28. Diersch S, et al. Kras(G12D) induces EGFR-MYC cross signaling in murine primary pancreatic ductal epithelial cells. *Oncogene*. 2016;35(29):3880–3886.
29. Walz S, et al. Activation and repression by oncogenic MYC shape tumour-specific gene expression profiles. *Nature*. 2014;511(7510):483–487.
30. Carrière C, Young AL, Gunn JR, Longnecker DS, Korc M. Acute pancreatitis markedly accelerates pancreatic cancer progression in mice expressing oncogenic Kras. *Biochem Biophys Res Commun*. 2009;382(3):561–565.
31. Guerra C, et al. Chronic pancreatitis is essential for induction of pancreatic ductal adenocarcinoma by K-Ras oncogenes in adult mice. *Cancer Cell*. 2007;11(3):291–302.
32. Caldwell ME, et al. Cellular features of senescence during the evolution of human and murine ductal pancreatic cancer. *Oncogene*. 2012;31(12):1599–1608.
33. Lesina M, et al. RelA regulates CXCL1/CXCR2-dependent oncogene-induced senescence in murine Kras-driven pancreatic carcinogenesis. *J Clin Invest*. 2016;126(8):2919–2932.
34. Bardeesy N, et al. Both p16(Ink4a) and the p19(Arf)-p53 pathway constrain progression of pancreatic adenocarcinoma in the mouse. *Proc Natl Acad Sci USA*. 2006;103(15):5947–5952.
35. Morton JP, et al. Mutant p53 drives metastasis and overcomes growth arrest/senescence in pancreatic cancer. *Proc Natl Acad Sci USA*. 2010;107(1):246–251.
36. Coppé JP, Desprez PY, Krtolica A, Campisi J. The senescence-associated secretory phenotype: the dark side of tumor suppression. *Annu Rev Pathol*. 2010;5:99–118.
37. Boj SF, et al. Organoid models of human and mouse ductal pancreatic cancer. *Cell*. 2015;160(1-2):324–338.
38. Moreira L, Bakir B, Chatterji P, Dantes Z, Reichert M, Rustgi AK. Pancreas 3D Organoids: Current and Future Aspects as a Research Platform for Personalized Medicine in Pancreatic Cancer. *Cell Mol Gastroenterol Hepatol*. 2018;5(3):289–298.
39. Reichert M, et al. Regulation of Epithelial Plasticity Determines Metastatic Organotropism in Pancreatic Cancer. *Dev Cell*. 2018;45(6):696–711.e8.
40. Rajput C, et al. Neural Wiskott-Aldrich syndrome protein (N-WASP)-mediated p120-catenin interaction with Arp2-Actin complex stabilizes endothelial adherens junctions. *J Biol Chem*. 2013;288(6):4241–4250.
41. Ramesh N, Antón IM, Hartwig JH, Geha RS. WIP, a protein associated with wiskott-aldrich syndrome protein, induces actin polymerization and redistribution in lymphoid cells. *Proc Natl Acad Sci USA*. 1997;94(26):14671–14676.
42. Azzolin L, et al. YAP/TAZ incorporation in the β-catenin destruction complex orchestrates the Wnt response. *Cell*. 2014;158(1):157–170.
43. Daniel JM. Dancing in and out of the nucleus: p120(ctn) and the transcription factor Kaiso. *Biochim Biophys Acta*. 2007;1773(1):59–68.
44. Daniel JM, Reynolds AB. The catenin p120(ctn) interacts with Kaiso, a novel BTB/POZ domain zinc finger transcription factor. *Mol Cell Biol*. 1999;19(5):3614–3623.
45. Daniel JM, Spring CM, Crawford HC, Reynolds AB, Baig A. The p120(ctn)-binding partner Kaiso is a bi-modal DNA-binding protein that recognizes both a sequence-specific consensus and methylated CpG dinucleotides. *Nucleic Acids Res*. 2002;30(13):2911–2919.
46. Iioka H, Doerner SK, Tamai K. Kaiso is a bimodal modulator for Wnt/beta-catenin signaling. *FEBS Lett*. 2009;583(4):627–632.
47. Blattler A, Yao L, Wang Y, Ye Z, Jin VX, Farnham PJ. ZBTB33 binds unmethylated regions of the genome associated with actively expressed genes. *Epigenetics Chromatin*. 2013;6(1):13.
48. Pierre CC, Hercules SM, Yates C, Daniel JM. Dancing from bottoms up - Roles of the POZ-ZF transcription factor Kaiso in Cancer. *Biochim Biophys Acta Rev Cancer*. 2019;1871(1):64–74.
49. van de Ven RA, Tenhagen M, Meuleman W, van Riel JJ, Schackmann RC, Derksen PW. Nuclear p120-catenin regulates the anoikis resistance of mouse lobular breast cancer cells through Kaiso-dependent Wnt11 expression. *Dis Model Mech*. 2015;8(4):373–384.
50. Schenk M, Aykut B, Teske C, Giese NA, Weitz J, Welsch T. Salinomycin inhibits growth of pancreatic cancer and cancer cell migration by disruption of actin stress fiber integrity. *Cancer Lett*. 2015;358(2):161–169.
51. Pieters T, et al. p120 Catenin-Mediated Stabilization of E-Cadherin Is Essential for Primitive Endoderm Specification. *PLoS Genet*. 2016;12(8):e1006243.
52. Zheng Y, et al. FAK phosphorylation by ERK primes ras-induced tyrosine dephosphorylation of FAK mediated by PIN1 and PTP-PEST. *Mol Cell*. 2009;35(1):11–25.
53. Taylor MD, et al. Nuclear role of WASp in the pathogenesis of dysregulated TH1 immunity in human Wiskott-Aldrich syndrome. *Sci Transl Med*. 2010;2(37):37ra44.
54. Benesch S, et al. N-WASP deficiency impairs EGF internalization and actin assembly at clathrin-coated pits. *J Cell Sci*. 2005;118(Pt 14):3103–3115.
55. Morris HT, et al. Loss of N-WASP drives early progression in an Apc model of intestinal tumourigenesis. *J Pathol*. 2018;245(3):337–348.
56. Russo JW, Castellot JJ. CCN5: biology and pathophysiology. *J Cell Commun Signal*. 2010;4(3):119–130.
57. Grunberg JR, Hammarstedt A, Hedjazifar S, Smith U. The Novel Secreted Adipokine WNT1-inducible Signaling Pathway Protein 2 (WISP2) Is a Mesenchymal Cell Activator of Canonical WNT. *J Biol Chem*. 2014;289(10):6899–6907.
58. Shao DD, et al. KRAS and YAP1 converge to regulate EMT and tumor survival. *Cell*. 2014;158(1):171–184.
59. Khalafalla FG, Khan MW. Inflammation and Epithelial-Mesenchymal Transition in Pancreatic Ductal Adenocarcinoma: Fighting Against Multiple Opponents. *Cancer Growth Metastasis*. 2017;10:1179064417709287.
60. Wang S, Huang S, Sun YL. Epithelial-Mesenchymal Transition in Pancreatic Cancer: A Review. *Biomed Res Int*. 2017;2017:2646148.
61. Pylayeva-Gupta Y, Lee KE, Hajdu CH, Miller G, Bar-Sagi D. Oncogenic Kras-induced GM-CSF production promotes the development of pancreatic neoplasia. *Cancer Cell*. 2012;21(6):836–847.
62. Piccolo S, Dupont S, Cordenonsi M. The biology of YAP/TAZ: hippo signaling and beyond. *Physiol Rev*. 2014;94(4):1287–1312.
63. Vaduva G, et al. The human WASP-interacting protein, WIP, activates the cell polarity pathway in yeast. *J Biol Chem*.

1999;274(24):17103–17108.
64. García E, Machesky LM, Jones GE, Antón IM. WIP is necessary for matrix invasion by breast cancer cells. *Eur J Cell Biol*. 2014;93(10-12):413–423.
65. Wu W, et al. *Tp53* Mutation Inhibits Ubiquitination and Degradation of WISP1 via Down-Regulation of Siah1 in Pancreatic Carcinogenesis. *Front Pharmacol*. 2018;9:857.
66. Vinyoles M, et al. Multivesicular GSK3 sequestration upon Wnt signaling is controlled by p120-catenin/cadherin interaction with LRP5/6. *Mol Cell*. 2014;53(3):444–457.
67. Kelly KF, Otchere AA, Graham M, Daniel JM. Nuclear import of the BTB/POZ transcriptional regulator Kaiso. *J Cell Sci*. 2004;117(Pt 25):6143–6152.
68. Ardito CM, et al. EGF receptor is required for KRAS-induced pancreatic tumorigenesis. *Cancer Cell*. 2012;22(3):304–317.
69. Lommel S, Benesch S, Rottner K, Franz T, Wehland J, Kühn R. Actin pedestal formation by enteropathogenic Escherichia coli and intracellular motility of Shigella flexneri are abolished in N-WASP-defective cells. *EMBO Rep*. 2001;2(9):850–857.
70. Renz BW, et al. Cholinergic Signaling via Muscarinic Receptors Directly and Indirectly Suppresses Pancreatic Tumorigenesis and Cancer Stemness. *Cancer Discov*. 2018;8(11):1458–1473.
71. Ruess DA, et al. Mutant KRAS-driven cancers depend on PTPN11/SHP2 phosphatase. *Nat Med*. 2018;24(7):954–960.
72. Subramanian A, et al. Gene Set Enrichment Analysis: A Knowledge-Based Approach for Interpreting Genome-Wide Expression Profiles. *Proc Natl Acad Sci U S A*. 2005;102(43):15545–15550.
73. Liberzon A, Subramanian A, Pinchback R, Thorvaldsdóttir H, Tamayo P, Mesirov JP. Molecular Signatures Database (MSigDB) 3.0. *Bioinformatics*. 2011;27(12):1739–1740.
74. Goldman M, Craft B, Kamath A, Brooks A, Zhu J, Haussler D. The UCSC Xena Platform for cancer genomics data visualization and interpretation. https://doi.org/10.1101/326470. Posted on bioRxiv September 26, 2019.